Title

Optimizing the Solvent Reorganization Free Energy by Metal Substitution for Nanocage Catalysis

Journal

ACS Catalysis, 12(7)

ISSN

2155-5435

Authors

Li, Wan-Lu

Hao, Hongxia

Head-Gordon, Teresa

Publication Date

2022-04-01

DOI

10.1021/acscatal.1c05980

Optimizing the solvent reorganization free energy by metal substitution for nanocage catalysis

Wan-Lu Li,[†,‡,¶] Hongxia Hao,[†,‡,¶] and Teresa Head-Gordon[*,†,‡,¶,§,‖]

†*Kenneth S. Pitzer Center for Theoretical Chemistry, Berkeley, CA, USA.*

‡*Department of Chemistry, University of California, Berkeley, CA, USA.*

¶*Chemical Sciences Division, Lawrence Berkeley National Labs, Berkeley, CA, USA.*

§*Department of Chemical and Biomolecular Engineering, University of California, Berkeley, CA, USA.*

‖*Department of Bioengineering, University of California, Berkeley, CA, USA.*

Received February 16, 2022; E-mail: thg@berkeley.edu

Abstract: The supramolecular capsule $Ga_4L_6^{12-}$ has been found to catalyze a number of important chemical reactions, but the close proximity of a poorly organized external solvent environment can serve as an impediment to the reaction chemistry. Using *ab initio* molecular dynamic calculations and electric field analyses, we find that metal substitution of Indium for Gallium lowers the total and electrostatic activation barriers by 3-4 kcal/mol in water solvent. Using an energy decomposition analysis of the interaction of water solvent with the metal vertices, we find that Pauli repulsion between the metal and water decreases, allowing the water coordination with the metal to increase, upon substitution of In for Ga. We therefore determine that the stabilization of the transition state is due to a better arrangement of water molecules around the metal vertices of $In_4L_6^{12-}$, and provides a proof of concept of how to redesign the nanocage scaffold in order to reduce the solvent reorganization energy.

Keywords: nanocage catalysis, reorganization energy, electric field analysis, metal substitution, solvation

Supramolecular capsules are thermodynamically stable assemblies with hollow cavities [1–5] that can encapsulate water droplets,[6] small catalytic entities, and/or substrate molecules.[7] Metal-ligand assemblies such as $M_4L_6^{12-}$ have also been suggested to be a biomimetic catalyst,[8] segregating the reactive site center from the immediate solvent environment and closely adhering to Michaelis-Menten kinetics.[9–11] For the $Ga_4L_6^{12-}$ assembly that coordinates the metal with naphthalene organic spacers, experiment has shown that the dehalogenated form of a gold complex $(P(CH_3)_3(CH_3)_2Au^+$ segregates into the nanocage in pure methanol solvent (Figure 1a),[12] *that accelerates the* k_{cat}/k_{uncat} *of the alkyl-alkyl reductive elimination reaction (Figure 1b) by* 5.0×10^5 *to* 2.5×10^6, which is nonetheless modest by natural enzyme standards.

To understand the chemical stability and reaction mechanism of the $Ga_4L_6^{12-}$ assemblies, theoretical simulations have provided insight into the origin of their catalytic mechanisms. Ujaque and co-workers comprehensively studied the rate acceleration of alkyl-alkyl reductive elimination in the capsules in pure methanol solvent, which are under the same solvent conditions used in experiments.[13,14] They established the key factors that reduce the free energy barrier are the preference for encapsulation of the dehalogenated form of the gold complex and the detailed methanol microsolvation events inside the nanocage. Very recently, our group investigated the electrostatics of the $Ga_4L_6^{12-}$ assembly on the same catalytic reaction to understand the host-guest interaction in the presence of pure water solvent.[15] Using electric field analysis that determines whether there is good field alignment along reactive bonds, in this case the breaking Au-C and forming C-C bonds, we found that the Ga nanocage itself slightly promotes the reaction, but that the encapsulated water molecule contributes most to the rate acceleration through free energy stabilization of the transition state. This is similar to the case of enzymes, in which Warshel and co-workers have emphasized the importance of a protein scaffold evolutionarily designed for minimizing reorganization energy, and solvation substitution rather than desolvation, by reorienting the active site dipoles to better stabilize the TS in the enzyme than in the bulk water reaction.[16–19]

Furthermore, Welborn et al.[15] found that the bulk water environment around the $Ga_4L_6^{12-}$ cage was highly detrimental to the alkyl-alkyl reductive elimination reaction, destabilizing the transition state by $\sim$10 kcal/mol. Warshel introduced the concept of solvent pre-organization as the principal catalytic effect in enzymes, i.e. that enzymes correctly orient the active site dipoles (charge distribution) to stabilize the TS better than the RS. Although purported to be biomimetic, it is immediately apparent that the electrostatically "pre-organized" protein scaffold of an enzyme is lacking in the synthetic $Ga_4L_6^{12-}$ catalyst, in which the latter places the active site center closer to the bulk solvent that lacks such organization. Therefore there is an opportunity for better design of a supramolecular catalyst that can ameliorate the solvent reorganization cost to further accelerate the reaction, and is the main thrust of the work reported here.

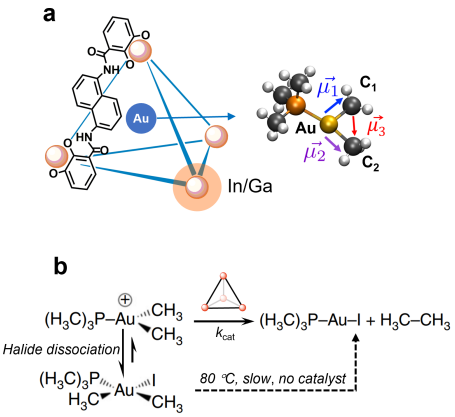

Figure 1. *The* $M_4L_6^{12-}$ *supramolecular capsule and mechanism of alkyl-alkyl reductive elimination reaction.* (a) Schematic structure of the $M_4L_6^{12-}$ cage (M = Ga, In; L = N,N'-bis(2,3-dihydroxybenzoyl)-1,5-diaminonaphtalene) encapsulating the central gold complex $P(CH_3)_3(CH_3)_2Au^+$. (b) Catalytic procedure of methyl-methyl reduction from the unhalogenated form of gold complex. Figure 1a adapted from reference.[12] Reprinted with permission from AAAS.

The $M_4L_6^{12-}$ assembly is known to be stable in both pure

methanol[12] and pure water[6] solvents, in which we have previously shown that an encapsulated water droplet of 9 ± 1 water molecules exhibits a distinctly different phase of water. However, the central gold complex $P(CH_3)_3(CH_3)_2Au^+$ is only viable in organic reagents such as methanol. Even so, how solvent behaves in and near these nanocage assemblies will be important for understanding other reactions beyond reductive elimination from a gold complex. Thus, the changes in catalytic performance depending on bulk solvent organization is examined for methanol (as per the experiment),[12] water, and methanol/water mixtures. Since it was previously reported that Ga is more catalytic than Si for alkyl-alkyl reductive elimination, which originates from its larger charge state,[20,21] we investigate whether metal substitutions with the same charge but larger metallicity can reduce the reorganization cost of the solvent environment to further achieve reaction rate improvement for alkyl-alkyl reductive elimination.

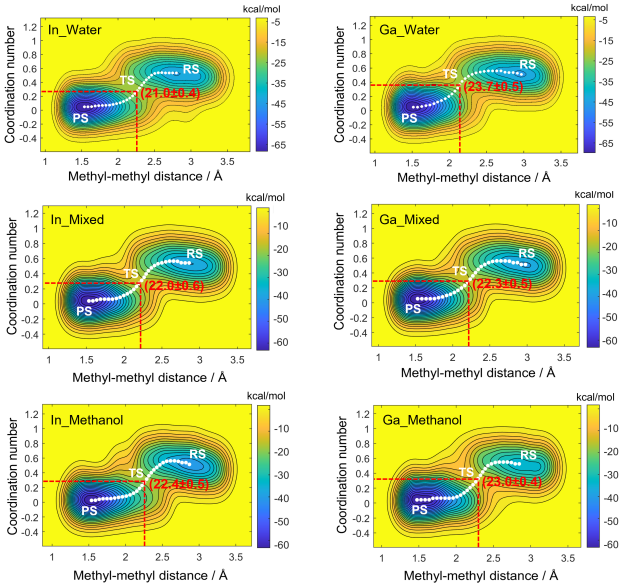

Figure 2. *Free energy landscapes for both $In_4L_6^{12-}$ (left) and $Ga_4L_6^{12-}$ (right) nanocages.* Free energies within the collective coordinates of Au coordination number and methyl-methyl distances obtained from ab initio metadynamics in (a) water, (b) mixed (85% methanol in volume), and (c) pure methanol solvents. The reaction starts from the reactant state (RS) in the top right corner to product state (PS) in the bottom left corner in each subplot. White dots define the minimum energy path using the zero-temperature string method. Red dots and values describe the positions of the transition state (TS) and free energy barrier in kcal/mol. Errors in the metadynamics simulation are estimated by the standard deviation of the last three recrossings.

We carried out AIMD metadynamic calculations for $Ga_4L_6^{12-}$ and $In_4L_6^{12-}$ in different solvent environments in order to obtain the free energy surfaces in the collective coordinates shown in Figure 2. Subsequent committor analysis confirmed that the putative transition state (TS) within the lower manifold was in fact the true TS in the full dimensional space. We find that the nanocages with different metal vertices in pure methanol (as per the experiment) or mixed methanol/water solvent demonstrate similar reaction barriers (< 1 kcal/mol difference in free energy). However we find a ∼3 kcal/mole reduction of the activation barrier for $In_4L_6^{12-}$ in water solvent compared to that calculated for the Ga metal, in principle giving rise to a rate acceleration of ~150 estimated from transition state theory with no recrossings.[22,23] Two orders of magnitude is potentially a significant improvement given the modest performance relative to enzymes of the original $Ga_4L_6^{12-}$ catalyst.

We have developed an approach for rationalizing catalytic reactions through electric field analysis.[24–27] With appropriate definitions of bond dipoles and electric fields of the transition state (TS) and reactant state (RS), we can estimate the free energy change in the activation barrier using Eq. (1)

$$\Delta G^{\dagger}_{elec} = -\sum_i \left\langle \boldsymbol{\mu}^i_{TS} \cdot \boldsymbol{E}^i_{TS} \right\rangle - \left\langle \boldsymbol{\mu}^i_{RS} \cdot \boldsymbol{E}^i_{RS} \right\rangle \qquad (1)$$

where $\boldsymbol{\mu}^i_X$ is the bond dipole of the breaking (or making) bond of interest, $\boldsymbol{E}^i_X$ is the electric field, and brackets denote an ensemble average over snapshots in the RS and TS ensembles. In this study, the sum is taken over the reactive Au–C1, Au–C2 and C1–C2 bonds of the gold complex to estimate the free energy from the bond dipole-field model[24] of both cages in different solvent environments. Consistent with the total free energy in Figure 2, the electrostatic free energy using Eq. (1) for the Ga metal differs by ∼1.0 kcal/mol in methanol or mixed solvent, and the electrostatic free energy for the In metal is negligibly different from Ga in the methanol solvents as seen in Table 1. However, in the more polar pure water environment we find that the In cage has nearly a ∼4 kcal/mol electrostatic free energy relative to Ga, indicating that the total free energy differences (Figure 2) arise mostly from differences in the electrostatics (Table 1).

To understand the electrostatic free energy changes due to differences in solvent and metal combinations for each supramolecular assembly, we have decomposed the electric field contributions by region, i.e. from the nanocage itself as well as for the solvent near the metal vertices or nanocage ligands, the encapsulated solvent, and the external bulk solvent. As seen in Table 1, although the nanocage itself provides TS stabilization through good electric field alignments with the catalytic complex, it is a more minor effect compared with the encapsulated solvent. According to the averaged geometries for both Ga and In nanocages, one water dimer, one methanol and one water, and one methanol is present near the gold complex with a permanent residence-time inside the

Table 1. *Electrostatic free energy contributions, $\Delta G^{\dagger}_{elec}$ calculated using Eq. (1) from different regions of the nanocage systems.* The total electrostatic free energy is comprised of the contributions from the encapsulated waters ($\Delta G^{\dagger}_{Encaps}$), the nanocage itself ($\Delta G^{\dagger}_{Cage}$), and solvent outside the nanocage, ($\Delta G^{\dagger}_{External}$). We further breakdown $\Delta G^{\dagger}_{External}$ into contributions from water near the metal vertices, near the organic ligand spacers, and from bulk water. Energy units are kcal/mol.

	$\Delta G^{\dagger}_{Encaps}$	$\Delta G^{\dagger}_{Cage}$	$\Delta G^{\dagger}_{External}$			$\Delta G^{\dagger}_{elec}$
			Near metal	Near ligand	Bulk	
Ga_Methanol	-10.97±0.92	-3.52±0.41	2.71±0.31	-0.06±0.01	1.56±0.12	-10.27±1.62
In_Methanol	-9.04±0.64	-2.87±0.22	1.83±0.19	0.18±0.00	1.03±0.00	-8.87±1.37
Ga_Mixed	-10.48±0.71	-3.38±0.70	1.41±0.11	0.46±0.00	3.07±0.22	-8.93±2.22
In_Mixed	-10.06±1.28	-3.09±0.72	0.12±0.01	-0.21±0.00	3.86±0.34	-9.38±2.98
Ga_Water	-12.77±0.92	-5.39±0.53	2.46±0.21	-1.16±0.09	6.85±0.66	-10.03±1.92
In_Water	-9.70±1.24	-3.41±0.36	-5.32±0.44	-1.89±0.13	6.21±0.59	-14.13±1.98

cage in pure water, mixed, and pure methanol solvent, respectively, for both RS (Figure S1) and TS (Figure 3). As we and others have previously reported for the pure water solvent and pure methanol solvent, these sequestered solvent molecules in the nanocages play the central catalytic role by reducing the activation energy for the reduction elimination reaction,[13–15,28] and this continues to be the case for the mixed water-methanol solvent and regardless of metal substitution. In particular, the nanocage geometry appears to enforce transition state geometries that are T-shape structures without strong bonding of the Au to the encapsulated solvent molecules, especially for those in mixed and pure methanol solvent. T-shape configurations are known to have a much lower energy barrier than the square-planar complex for reductive elimination,[29–31] and this is well-supported by our electric field analysis for $\Delta G^{\dagger}_{Encaps}$ in Table 1 (with more detail given in Tables S1-S3), where weaker bonding between the central gold and encapsulated solvent molecule induces more stabilization of the energy barrier to promote the reaction.

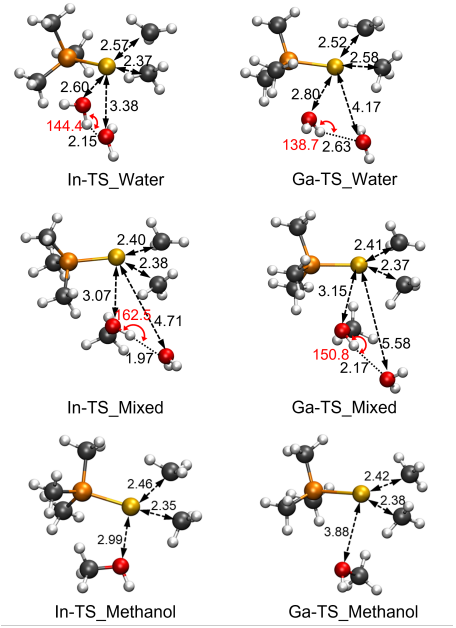

Figure 3. *Ensemble averaged geometries for the transition state of both In and Ga nanocages.* The simulation averaged geometric parameters (in units of Å, deg) are shown for Indium (left) and Gallium (right) capsules in pure water (top), mixture of 85% methanol and 15% water by volume (middle), and pure methanol solvent (bottom). Color key: carbon = grey, phosphorous = orange, gold = yellow, hydrogen = white, oxygen = red.

However, the electrostatic free energy due to the remaining solvent outside of the nanocages ($\Delta G^{\dagger}_{External}$) opposes the catalytic reaction. Figure 4a shows the further decomposition of the electric field of the external water environment into different regions: the first shell coordination near the organic ligands and near the metal vertices, and the remaining arising from bulk solvent. When these electric field components are projected onto the Au–C1, Au–C2 and C1–C2 reactive bonds to yield the electrostatic free energy contributions (Fig. 4b), we find no qualitative difference in solvation effects near the organic linkers or from bulk solvent between the two metal nanocages. However we find that the In nanocage creates a much more favorable solvent organization near the metal vertices that in turn gives rise to electric field alignments that promote the bond breaking of the Au–C1 and Au–C2 bonds. The substitution of In for Ga in water solvent induces a remarkably optimized microenvironment, stabilizing the TS by 7.8 kcal/mol as shown in Table 1, and largely is the origin of the TS free energy lowering for In vs. Ga seen in Figure 2.

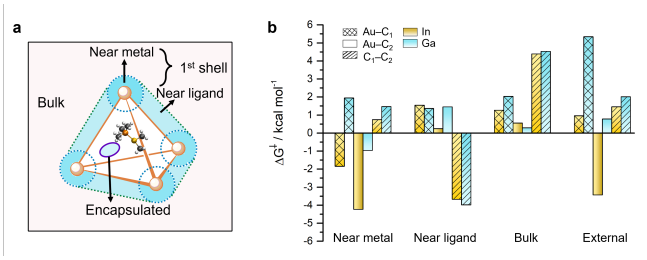

Figure 4. *Electrostatic free energy contributions of the external water environment.* (a) The regional definitions of different solvent environments (b) The electric fields in each region are projected onto the breaking Au-C1 and Au-C2 bonds and newly forming C1-C2 bond of the ethyl product in reductive elimination to yield free energies as given in Eq. (1), in kcal/mol. The negative free energy represents stabilization of the TS and enhancement of the catalytic effect. The external free energy is the sum of free energies from the near metal, near ligand, and bulk water regions. Figure S2 provides additional details.

To better address why the local water environment near the metal vertices organizes so differently in the two nanocapsules, we built a cluster model of the system (Figure 5a and 5b) to perform an energy decomposition analyses (EDA)[32–34] to determine the origin of energetic interactions between the metals and the nearby waters. The most recent ALMO-EDA approach[35] implemented in the Q-Chem package[36] decomposes the interaction energy between two fragments, in this case metal and water solvent, into electrostatic, Pauli repulsion, dispersion, polarization and charge-transfer terms. From the EDA analysis summarized in Figure 5c, we find that the In metal has a reduced Pauli repulsion with water, thereby increasing the water coordination to ~8.0, compared with ~6.8 for the Ga metal, as computed by integration under the first peak of the radial distribution function (see Fig. S2). This in turn creates a more favorable electrostatics, polarization, charge transfer, and dispersion interaction, and gives rise to a stronger total binding energy between the In metal and its more closely coordinated waters compared to that observed for the Ga metal.

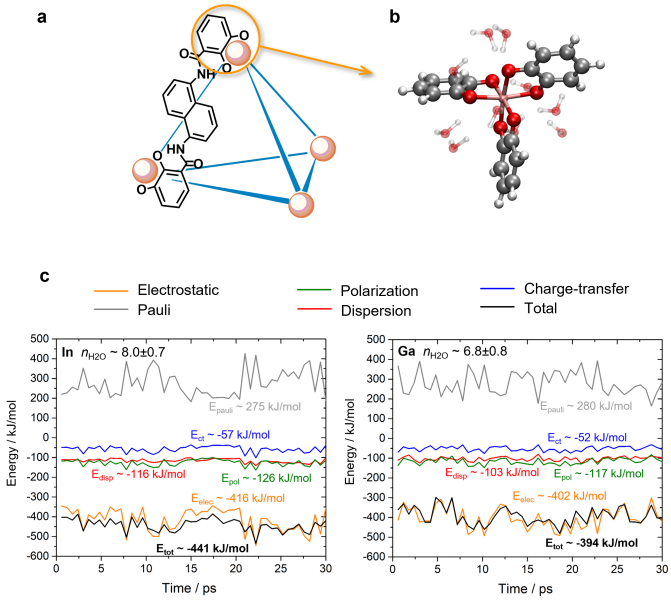

Figure 5. *Energy decomposition analysis for water molecules near the metal In and Ga vertices of the nanocage.* (a) the nanocage and (b) truncated metal ion cluster model. (c) EDA analyses[35] at the level of ωB97X-V hybrid functional[37] with def2-TZVP basis and its corresponding pseudopotential corrected by basis set superposition error[38] during 30 ps AIMD simulations. Herein, $E_{tot} = E_{elec} + E_{pauli} + E_{disp} + E_{pol} + E_{ct}$. Figure 5a adapted from reference.[12] Reprinted with permission from AAAS.

In summary, we have shown that metal substitution of Indium for

Gallium provides an acceleration rate of ~150 for carbon-carbon reductive elimination from a Au complex in a $M_4L_6^{12-}$ construct when examined under water solvent conditions. We find that the metal substitution weakens Pauli repulsion that in turn increases the first M-H_2O coordination shell with stronger electrostatic, polarization, and dispersion interactions. This change in solvent organization also improves the electric field projections from the external water solvent that promotes transitions state stabilization for breaking Au-C1 and Au-C2 bonds and forming the C1-C2 bond. Although this study considers a single reaction in a $M_4L_6^{12-}$ construct, we can reach more general conclusions about nanocage catalysis by considering their limitations with respect to enzyme biocatalysts. It has been purported that the nanocage sequesters the catalytic center away from solvent, but in fact it instead benefits directly from the incorporation of solvent molecules that are the primary catalytic entities. But the remaining solvent is still in close spatial proximity due to the fact that it is a nanocage, and the reorganization cost relative to the uncatalyzed reaction is not fully eliminated. While there may be other chemical reasons that methanol solvent was used for the carbon-carbon reductive elimination, it was also a fortuitous feature that the reorganization cost is lowest, albeit still unfavorable, among the 3 solvent conditions examined here. Thus to realize the promise of enzyme-like rate accelerations, the nanocage itself will require a redesign when generalized to new reactions and/or requiring different solvents such as water. Although we showed this was possible with metal substitution, we also note that changes in the ligand could also create a distinctive reorganized solvent environment to further accelerate chemical reactions, although this may be more difficult to achieve synthetically.

Supporting Information: Ensemble averaged geometries of RS and TS, definition of each region of the system, electric field results, density derived atomic charge and bond dipole results.

Acknowledgement We thank the CPIMS program, Office of Science, Office of Basic Energy Sciences, Chemical Sciences Division of the U.S. Department of Energy under Contract No. DE-AC02-05CH11231 for support. This work used computational resources provided by the National Energy Research Scientific Computing Center (NERSC), a U.S. Department of Energy Office of Science User Facility operated under Contract No. DE-AC02-05CH11231. WLL thanks Valerie Vaissier Welborn for helpful discussions on the electric field analyses and metadynamic simulations.

Theoretical methods. For a rational comparison of the catalytic character in both Indium and Gallium nanocages, we employed the same procedures and parameters in all the simulations, including ab initio molecular dynamics (AIMD), ab initio metadynamics, the zero-temperature string method, and committer analysis as we previously reported.[28] Herein we only introduce the changes in methods and models used in the Indium case.

Equilibration of the $M_4L_6^{12-}$ structure. The initial starting geometry of the gold cation complex encapsulated in the $In_4L_6^{12-}$ cage was created by replacing Ga atoms in our previous simulation with In atoms. We first optimized the structure in the gas phase with the dispersion corrected meta-GGA functional B97M-rV[39,40] and DZVP[41] basis sets as implemented in the CP2K software.[42,43] The stabilized structure was further solvated and neutralized by potassium counter cations. We then performed 5 ps AIMD simulations in order to collect 200 snapshots to define the reactant state (RS) ensembles. For the mixed solvent construction with a methanol volume ratio of 85%, we first performed 3 ns of equilibration in the NVT ensemble, followed by 3 ns simulation in the NPT ensemble with 50×50×50 box size using the AMOEBA polarized force field[44,45] implemented in the Tinker software package.[44,46,47] The nanocage and gold complex were then inserted into the solvent environment using utilities in the Gromacs software package.[48]

Ab initio metadynamics. In the well-tempered single walker metadynamic simulation,[49,50] over 40 ps was gathered for each system until the barrier was crossed more than five times between reactant and product wells. Since the mechanism of the reductive elimination reaction involves breaking the Au–C1/C2 bonds and bond formation of C1–C2, we utilized two collective variables (CVs) describing the evolution of the reaction as per our previous study on $Ga_4L_6^{12-}$,[15] i.e. the coordination number between Au and two C atoms and methyl-methyl distance. Umbrella sampling[51] simulations were carried out with 0.2 fs time step in the collective variables area (2.30 ± 0.01, 0.28 ± 0.01), generated by the zero-temperature string method[52] for determining the minimum paths. The force constant for the harmonic restraint k is set as 10 N/m. Until reaching the equilibrium within the defined region, we gathered 50 geometries for the TS ensembles of In catalyzed system, which are further verified and refined by committer analyses statistics.

Electric fields and bond dipole moments. We treated the two solvent molecules inside the cage together, instead of assigning the furthest water from the Au complex as bulk water as what we did for Ga nanocage in previous work.[?] The bond dipole moments of the reactive bonds Au–C1, Au–C2, and C1-C2 were computed using the density derived atomic point charge (DDAPC)[53] and are provided in Tables S4-S6.

Cluster model construction. AIMD simulations were performed on Indium and Gallium nanocage systems in water solvent without the central gold complex to generate a cluster model for the nanocage metal vertices. In our previous work on the water behavior of the nanocage system,[6] we found that the interfacial water properties show no difference with or without the encapsulated substrate (Et_4N^+ in that study).[6] Therefore we have simulated the nanocage without the Au complex to study the interaction between the metal and the water molecules in close proximity. After 5 ps of equilibration, we selected 50 snapshots from the 30 ps production simulation, onto which the structure at the metal vertex of the cage was truncated, saturated with hydrogen atoms, as illustrated in Figure 4 of the main text. Water molecules near the metals were determined from the radial distribution function as shown in Figure S2, and the first solvation shell included as a fragment to do the energy decomposition analysis.

Energy Decomposition Analysis. We performed an ALMO-EDA calculation[35] using the Q-Chem package[36] with the B97M-rV functional[39,40] in conjunction with def2-TZVP basis and its corresponding pseudopotential.[54,55] The total interaction energy (ΔE_{tot}) between the defined fragments is decomposed into five energy terms, viz., electrostatic interaction (ΔE_{elec}), Pauli repulsion (ΔE_{Pauli}), dispersion interaction (ΔE_{disp}), polarization (ΔE_{pol}) and charge-transfer energy (ΔE_{CT}), where the first three terms together describe the interaction of the isolated fragment densities aggregated, (ΔE_{pol}) is obtained by variationally optimizing the localized wave function, and the charge-transfer energy (ΔE_{CT}) is determined as the remainder after subtraction of these components from the total energy (ΔE_{tot}).

$$\Delta E_{tot} = \Delta E_{elec} + \Delta E_{Pauli} + \Delta E_{disp} + \Delta E_{pol} + \Delta E_{CT} \quad (2)$$

References

(1) Klöck, C.; Dsouza, R. N.; Nau, W. M. Cucurbituril-Mediated Supramolecular Acid Catalysis. *Org. Lett.* **2009**, *11*, 2595–2598, PMID: 19462966.
(2) Szejtli, J. Introduction and General Overview of Cyclodextrin Chemistry. *Chem. Rev.* **1998**, *98*, 1743–1754, PMID: 11848947.

(3) Schneider, H.-J.; Hacket, F.; Rüdiger, V.; Ikeda, H. NMR Studies of Cyclodextrins and Cyclodextrin Complexes. *Chemical Reviews* **1998**, *98*, 1755–1786, PMID: 11848948.
(4) Ikeda, A.; Shinkai, S. Novel Cavity Design Using Calix[n]arene Skeletons: Toward Molecular Recognition and Metal Binding. *Chem. Rev.* **1997**, *97*, 1713–1734, PMID: 11851464.
(5) Schühle, D. T.; Peters, J. A.; Schatz, J. Metal binding calixarenes with potential biomimetic and biomedical applications. *Coord. Chem. Rev.* **2011**, *255*, 2727–2745.
(6) Sebastiani, F.; Bender, T. A.; Pezzotti, S.; Li, W.-L.; Schwaab, G.; Bergman, R. G.; Raymond, K. N.; Toste, F. D.; Head-Gordon, T.; Havenith, M. An isolated water droplet in the aqueous solution of a supramolecular tetrahedral cage. *Proc. Natl. Acad. Sci. U.S.A.* **2020**, *117*, 32954–32961.
(7) Koblenz, T. S.; Wassenaar, J.; Reek, J. N. H. Reactivity within a confined self-assembled nanospace. *Chem. Soc. Rev.* **2008**, *37*, 247–262.
(8) Wiester, M. J.; Ulmann, P. A.; Mirkin, C. A. Enzyme mimics based upon supramolecular coordination chemistry. *Angew. Chem. Int. Ed.* **2011**, *50*, 114–37.
(9) Michaelis, L.; Menten, M. M. L. The kinetics of invertin action. *FEBS Letters* **2013**, *587*, 2712–2720.
(10) Levin, M. D.; Kaphan, D. M.; Hong, C. M.; Bergman, R. G.; Raymond, K. N.; Toste, F. D. Scope and Mechanism of Cooperativity at the Intersection of Organometallic and Supramolecular Catalysis. *J. Am. Chem. Soc.* **2016**, *138*, 9682–9693, PMID: 27458778.
(11) Hong, C. M.; Kaphan, D. M.; Bergman, R. G.; Raymond, K. N.; Toste, F. D. Conformational Selection as the Mechanism of Guest Binding in a Flexible Supramolecular Host. *J. Am. Chem. Soc.* **2017**, *139*, 8013–8021, PMID: 28581740.
(12) Kaphan, D. M.; Levin, M. D.; Bergman, R. G.; Raymond, K. N.; Toste, F. D. A supramolecular microenvironment strategy for transition metal catalysis. *Science* **2015**, *350*, 1235–1238.
(13) Norjmaa, G.; Maréchal, J.-D.; Ujaque, G. Microsolvation and Encapsulation Effects on Supramolecular Catalysis: C–C Reductive Elimination inside [Ga4L6]12– Metallocage. *J. Am. Chem. Soc.* **2019**, *141*, 13114–13123, PMID: 31390202.
(14) Norjmaa, G.; Maréchal, J.-D.; Ujaque, G. Reaction Rate Inside the Cavity of [Ga4L6]12 Supramolecular Metallocage is Regulated by the Encapsulated Solvent. *Chem. Eur. J.* **2020**, *26*, 6988–6992.
(15) Welborn, V. V.; Li, W.-L.; Head-Gordon, T. Interplay of water and a supramolecular capsule for catalysis of reductive elimination reaction from gold. *Nat. Commun.* **2020**, *11*, 415.
(16) Warshel, A. Energetics of enzyme catalysis. *Proc. Natl. Acad. Sci. U.S.A.* **1978**, *75*, 5250–5254.
(17) Warshel, A.; Aqvist, J.; Creighton, S. Enzymes work by solvation substitution rather than by desolvation. *Proc. Natl. Acad. Sci. U.S.A.* **1989**, *86*, 5820–5824.
(18) Villà, J.; Warshel, A. Energetics and Dynamics of Enzymatic Reactions. *J. Phys. Chem. B* **2001**, *105*, 7887–7907.
(19) Warshel, A.; Sharma, P. K.; Kato, M.; Xiang, Y.; Liu, H.; Olsson, M. H. M. Electrostatic Basis for Enzyme Catalysis. *Chem. Rev.* **2006**, *106*, 3210–3235, PMID: 16895325.
(20) Vaissier Welborn, V.; Head-Gordon, T. Electrostatics Generated by a Supramolecular Capsule Stabilizes the Transition State for Carbon–Carbon Reductive Elimination from Gold(III) Complex. *J. Phys. Chem. Lett.* **2018**, *9*, 3814–3818.
(21) Stelson, A. C.; Hong, C. M.; Groenenboom, M. C.; Little, C. A. E.; Booth, J. C.; Orloff, N. D.; Bergman, R. G.; Raymond, K. N.; Schwarz, K. A.; Toste, F. D.; Long, C. J. Measuring ion-pairing and hydration in variable charge supramolecular cages with microwave microfluidics. *Commun. Chem.* **2019**, *2*, 54.
(22) Eyring, H. The Activated Complex in Chemical Reactions. *J. Chem. Phys.* **1935**, *3*, 107–115.
(23) Truhlar, D. G.; Garrett, B. C.; Klippenstein, S. J. Current Status of Transition-State Theory. *J. Phys. Chem.* **1996**, *100*, 12771–12800.
(24) Bhowmick, A.; Sharma, S. C.; Head-Gordon, T. The Importance of the Scaffold for de Novo Enzymes: A Case Study with Kemp Eliminase. *Journal of the American Chemical Society* **2017**, *139*, 5793–5800, PMID: 28383910.
(25) Welborn, V. V.; Ruiz Pestana, L.; Head-Gordon, T. Computational optimization of electric fields for better catalysis design. *Nat. Catal.* **2018**, *1*, 649–655.
(26) Vaissier Welborn, V.; Head-Gordon, T. Computational Design of Synthetic Enzymes. *Chem. Rev.* **2019**, *119*, 6613–6630, PMID: 30277066.
(27) Li, W.-L.; Head-Gordon, T. Catalytic Principles from Natural Enzymes and Translational Design Strategies for Synthetic Catalysts. *ACS Cent. Sci.* **2021**, *7*, 72–80.
(28) Welborn, V. V.; Li, W.-L.; Head-Gordon, T. Interplay of water and a supramolecular capsule for catalysis of reductive elimination reaction from gold. *Nat. Commun.* **2020**, *11*, 415.
(29) Tatsumi, K.; Hoffmann, R.; Yamamoto, A.; Stille, J. K. Reductive Elimination of d8-Organotransition Metal Complexes. *Bull. Chem. Soc. Jpn.* **1981**, *54*, 1857–1867.
(30) Pérez-Rodríguez, M.; Braga, A. A. C.; Garcia-Melchor, M.; Pérez-Temprano, M. H.; Casares, J. A.; Ujaque, G.; de Lera, A. R.; Álvarez, R.; Maseras, F.; Espinet, P. CC Reductive Elimination in Palladium Complexes, and the Role of Coupling Additives. A DFT Study Supported by Experiment. *J. Am. Chem. Soc* **2009**, *131*, 3650–3657, PMID: 19231862.
(31) Ananikov, V. P.; Musaev, D. G.; Morokuma, K. Critical Effect of Phosphane Ligands on the Mechanism of Carbon–Carbon Bond Formation Involving Palladium(II) Complexes: A Theoretical Investigation of Reductive Elimination from Square-Planar and T-Shaped Species. *Eur. J. Inorg. Chem.* **2007**, *2007*, 5390–5399.
(32) Su, P.; Li, H. Energy decomposition analysis of covalent bonds and intermolecular interactions. *J. Chem. Phys.* **2009**, *131*, 014102.
(33) Hopffgarten, M. v.; Frenking, G. Energy decomposition analysis. *WIREs Comput. Mol. Sci.* **2012**, *2*, 43–62.
(34) Mao, Y.; Loipersberger, M.; Horn, P. R.; Das, A.; Demerdash, O.; Levine, D. S.; Prasad Veccham, S.; Head-Gordon, T.; Head-Gordon, M. From Intermolecular Interaction Energies and Observable Shifts to Component Contributions and Back Again: A Tale of Variational Energy Decomposition Analysis. *Annual Review of Physical Chemistry* **2021**, *72*, 641–666, PMID: 33636998.
(35) Horn, P. R.; Mao, Y.; Head-Gordon, M. Probing non-covalent interactions with a second generation energy decomposition analysis using absolutely localized molecular orbitals. *Phys. Chem. Chem. Phys.* **2016**, *18*, 23067–23079.
(36) Epifanovsky, E. et al. Software for the frontiers of quantum chemistry: An overview of developments in the Q-Chem 5 package. *J. Chem. Phys.* **2021**, *155*, 084801.
(37) Mardirossian, N.; Head-Gordon, M. ωB97X-V: A 10-parameter, range-separated hybrid, generalized gradient approximation density functional with nonlocal correlation, dsigned by a survival-of-the-fittest strategy. *Phys. Chem. Chem. Phys.* **2014**, *16*, 9904–9924.
(38) Balabin, R. M. Enthalpy difference between conformations of normal alkanes: Intramolecular basis set superposition error (BSSE) in the case of n-butane and n-hexane. *J. Chem. Phys.* **2008**, *129*, 164101.
(39) Mardirossian, N.; Head-Gordon, M. Mapping the genome of meta-generalized gradient approximation density functionals: The search for B97M-V. *J. Chem. Phys.* **2015**, *142*, 074111.
(40) Mardirossian, N.; Head-Gordon, M. Thirty years of density functional theory in computational chemistry: an overview and extensive assessment of 200 density functionals. *Mol. Phys.* **2017**, *115*, 2315–2372.
(41) VandeVondele, J.; Hutter, J. Gaussian basis sets for accurate calculations on molecular systems in gas and condensed phases. *J. Chem. Phys.* **2007**, *127*, 114105.
(42) Hutter, J.; Iannuzzi, M.; Schiffmann, F.; VandeVondele, J. cp2k: atomistic simulations of condensed matter systems. *WIREs Comput. Mol. Sci.* **2014**, *4*, 15–25.
(43) VandeVondele, J.; Krack, M.; Mohamed, F.; Parrinello, M.; Chassaing, T.; Hutter, J. Quickstep: Fast and accurate density functional calculations using a mixed Gaussian and plane waves approach. *Comput. Phys. Commun.* **2005**, *167*, 103–128.
(44) Ponder, J. W.; Wu, C.; Ren, P.; Pande, V. S.; Chodera, J. D.; Schnieders, M. J.; Haque, I.; Mobley, D. L.; Lambrecht, D. S.; DiStasio, R. A.; Head-Gordon, M.; Clark, G. N. I.; Johnson, M. E.; Head-Gordon, T. Current Status of the AMOEBA Polarizable Force Field. *J. Phys. Chem. B* **2010**, *114*, 2549–2564, PMID: 20136072.
(45) Ren, P.; Wu, C.; Ponder, J. W. Polarizable Atomic Multipole-Based Molecular Mechanics for Organic Molecules. *J. Chem. Theory and Comput.* **2011**, *7*, 3143–3161, PMID: 22022236.
(46) Ponder, J. W. Tinker–Software Tools for Molecular Design, 7.0. **2014**,
(47) Albaugh, A. et al. Advanced Potential Energy Surfaces for Molecular Simulation. *J. Phys. Chem. B* **2016**, *120*, 9811–9832, PMID: 27513316.
(48) Abraham, M. J.; Murtola, T.; Schulz, R.; Páll, S.; Smith, J. C.; Hess, B.; Lindahl, E. GROMACS: High performance molecular simulations through multi-level parallelism from laptops to supercomputers. *SoftwareX* **2015**, *1-2*, 19–25.
(49) Barducci, A.; Bussi, G.; Parrinello, M. Well-Tempered Metadynamics: A Smoothly Converging and Tunable Free-Energy Method. *Phys. Rev. Lett.* **2008**, *100*, 020603.
(50) Barducci, A.; Bonomi, M.; Parrinello, M. Metadynamics. *WIREs Comput. Mol. Sci.* **2011**, *1*, 826–843.
(51) Kästner, J. Umbrella sampling. *WIREs Comput. Mol. Sci.* **2011**, *1*, 932–942.
(52) Maragliano, L.; Fischer, A.; Vanden-Eijnden, E.; Ciccotti, G. String method in collective variables: Minimum free energy paths and isocommittor surfaces. *J. Chem. Phys.* **2006**, *125*, 024106.
(53) Blöchl, P. E. Electrostatic decoupling of periodic images of plane-wave-expanded densities and derived atomic point charges. *J. Chem. Phys.* **1995**, *103*, 7422–7428.
(54) Rappoport, D.; Furche, F. Property-optimized Gaussian basis sets for molecular response calculations. *The Journal of Chemical Physics* **2010**, *133*, 134105.
(55) Weigend, F.; Ahlrichs, R. Balanced basis sets of split valence, triple zeta valence and quadruple zeta valence quality for H to Rn: Design and assessment of accuracy. *Phys. Chem. Chem. Phys.* **2005**, *7*, 3297–3305.

TOC Graphic

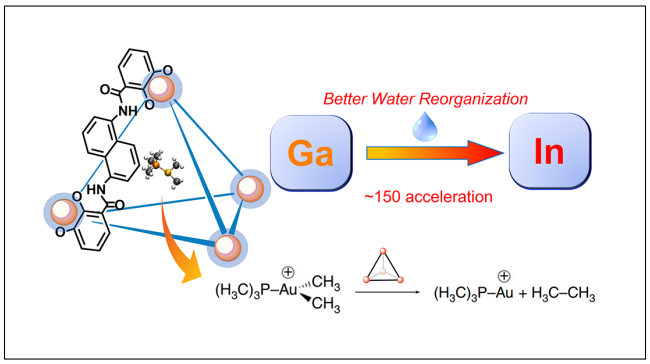
Better Water Reorganization
Ga
In
~150 acceleration
(H3C)3P–Au
CH3
CH3
(H3C)3P–Au + H3C–CH3